SOME ASPECTS OF FORECAST AND MODEL ERROR

Herschel Mitchell[1], Roger Daley[2] and Peter Bartello[1]

[1]Recherche en prévision numérique, Dorval, Québec,

[2]Canadian Climate Centre, Downsview, Ontario

Canada

Abstract: Two topics are dealt with in this paper. First, a continuous three-dimensional model of short-range forecast error covariances is described. Unlike commonly-used representations, this model does not assume vertical/horizontal separability. Second, some results of a study of the effect of assimilating model resolution on data assimilation are presented.

1. A CONTINUOUS THREE-DIMENSIONAL COVARIANCE MODEL

Due to its importance for data assimilation, considerable effort has been expended over the past several decades on studying and modelling the structure of short-range forecast-error covariances. Most commonly used representations assume vertical/horizontal separability of these covariances, although the studies of Hollingsworth and Lönnberg (1986; hereafter HL), Lönnberg and Hollingsworth (1986; hereafter LH), and Mitchell et al. (1990) have indicated deficiencies with this assumption. In particular, the observed significant increase with height of horizontal decorrelation length scales cannot be represented.

A three-dimensional representation of the structure of forecast error covariances has been developed using archived observed residuals, or differences, between the short-range forecasts used as trial fields in an operational data assimilation system and the verifying radiosonde data. Assuming homogeneity and isotropy on pressure surfaces, geopotential and wind covariances were fitted to a series expansion employing zero-order Bessel functions of the first kind, J_0, as the horizontal basis functions (Gandin, 1963; Rutherford, 1972) and the normal modes of the primitive equations, $A_n(Z)$, as the vertical basis functions (Phillips, 1986), i.e.

$$\left\langle \phi(\mathbf{r},Z_1,t)\ \phi(\mathbf{r}+\mathbf{s},Z_2,t) \right\rangle = B(s,Z_1,Z_2) = \sum_{n,m,j} \widehat{B}_{nmj}\, A_n(Z_1)\, A_m(Z_2)\, J_0(\kappa_j s) \quad , \qquad (1)$$

where ϕ represents the error field, $\mathbf{r} = x\boldsymbol{i} + y\boldsymbol{j}$, $s = |\mathbf{s}|$ is the horizontal separation, and $Z = -H \ln(p/p_s)$ is the vertical coordinate. Rather than discretize horizontally by imposing a Neumann boundary condition at large separation (Rutherford, 1972; HL/LH), we have used a Dirichlet condition in order to avoid large-scale/synoptic-scale partitioning of the results. Therefore the κ_j were selected such that $J_0(\kappa_j L) = 0$, where $L = 0.6$ radians (~ 3800 km).

The formulation is similar to that proposed by Phillips (1986) except that: (1) rather than assume equipartition of forecast error energy, the appropriate spectral distribution has been determined via a direct fitting procedure, (2) horizontal isotropy has been assumed, permitting the use of a single Fourier-Bessel series expansion in place of double Fourier sums, and (3) the closed analytical form for $A_n(Z)$, made possible by the vertical log-pressure coordinate and the isothermal basic state, results in a spatially continuous function. This allows for the calculation of the covariance between any two points in three-dimensional space. Unlike commonly-used representations employing vertical/horizontal separability, the present model reproduces the observed significant increase of horizontal decorrelation length scales with height.

The model has been used to examine covariances of geopotential as well as transverse and longitudinal wind components. The wind data have been used to obtain divergent and solenoidal components and subsequent comparison of stream function and geopotential statistics has revealed a high degree of geostrophic balance away from the upper and lower boundaries. This can be seen from Fig. 1 and by comparing Fig. 2 (geopotential) and Fig. 3 (stream function).

Assuming the wind components to be diagnostically related to the geopotential field via the quasi-geostrophic assumption, various cross-correlations can be computed. In Fig. 4 we display the geostrophically-derived uu , uv and $u\phi$ correlations on the x-y plane at three different levels. Other velocity/geopotential correlations are simply related to these via appropriate rotations or reflections. The horizontal spatial structure of the correlation changes with height in a manner consistent with the archived geopotential statistics. The 500 mb correlations can be directly compared with those in Fig. 17 of Mitchell et al. (1990), which were obtained from a horizontal correlation representation based on a sum of autoregressive functions. Such a comparison indicates very good agreement.

The correlations in Fig. 4 are obtained with $Z_1 = Z_2$. The model can also be used to examine the influence of a single datum at other levels. In Fig. 5 we display the geostrophically-derived correlations generated by a single u -residual at Z_1 corresponding to 500 mb with Z_2 at the 250, 500 and 700 mb levels. The 500-850 mb correlations (not shown) were very small, with uu and uv not even attaining a value of 0.1. Clearly evident from Fig. 5 are the diminished correlations at $Z_2 \neq Z_1$. The unusual double negative lobes of the 500-250 mb uu correlation reflect the shape of the uu correlation at 250 mb in Fig. 4.

A detailed description of the three-dimensional covariance model and the results obtained can be found in Bartello and Mitchell (1992). The model is currently being implemented in a statistical interpolation procedure with a view to assessing the benefits of a non-separable forecast-error representation.

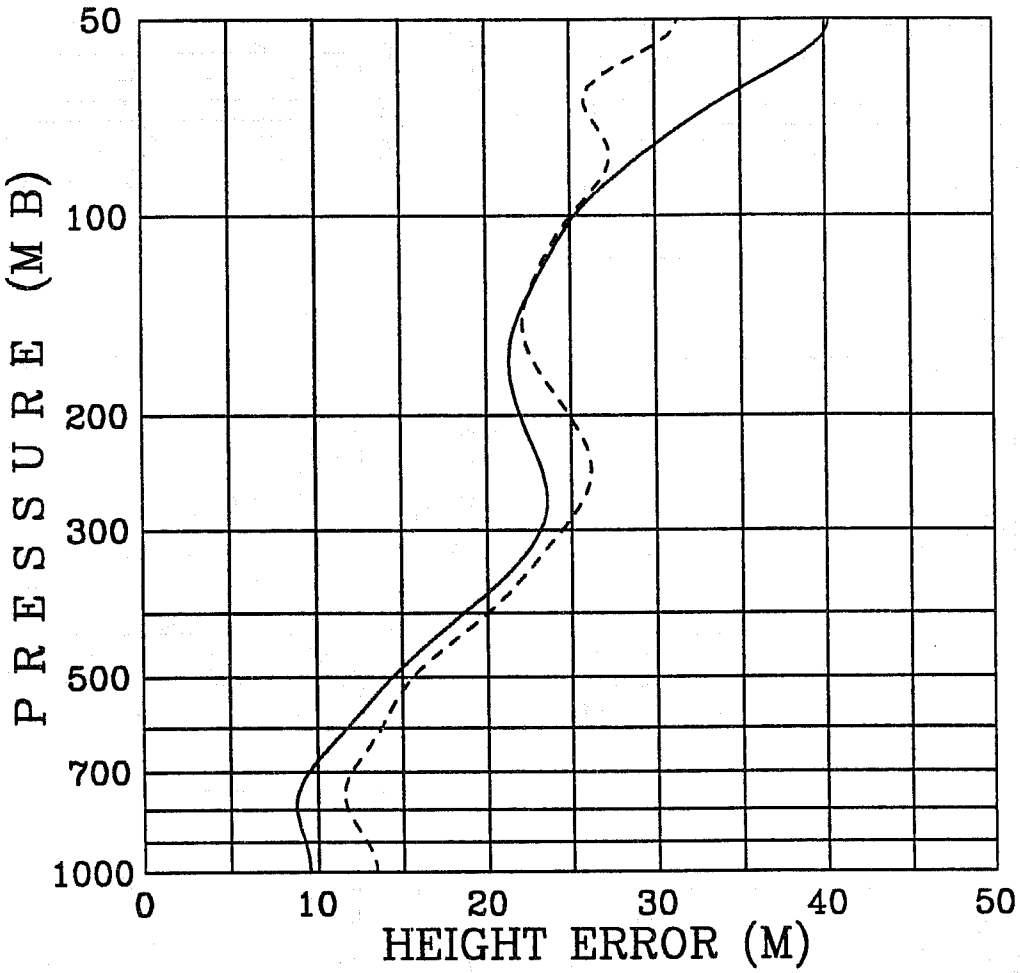

Fig. 1. Root mean square height prediction error (m) as derived from the geopotential, (ϕ/g) (solid line) and from the stream function assuming geostrophy, ($f\psi$ / g) (dashed line) as a function of *Z*.

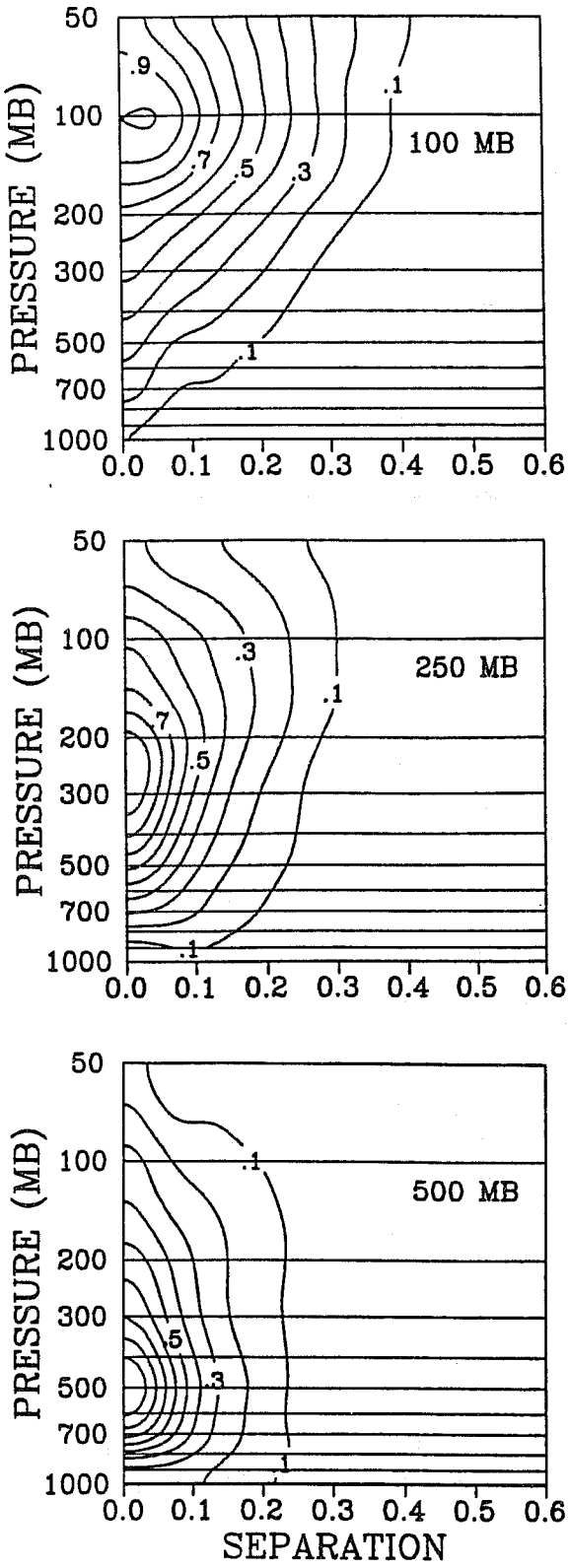

Fig. 2. Geopotential error correlations at three selected levels corresponding to 100, 250, and 500 mb, contoured on the *Z-s* plane, where *s* is measured in radians. Since the fields contain small-scale, low-amplitude oscillations at large separations, the zero contour has been omitted.

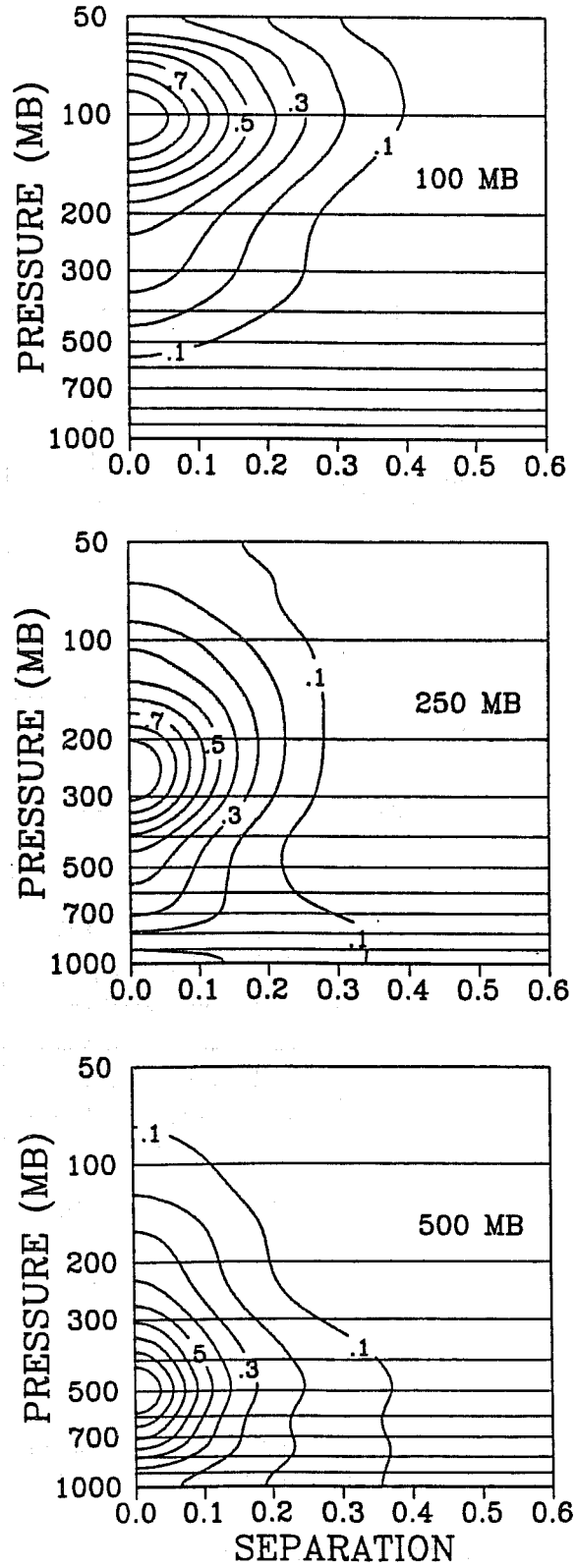

Fig. 3.The velocity stream function correlation at 100, 250 and 500 mb as in Fig. 2.

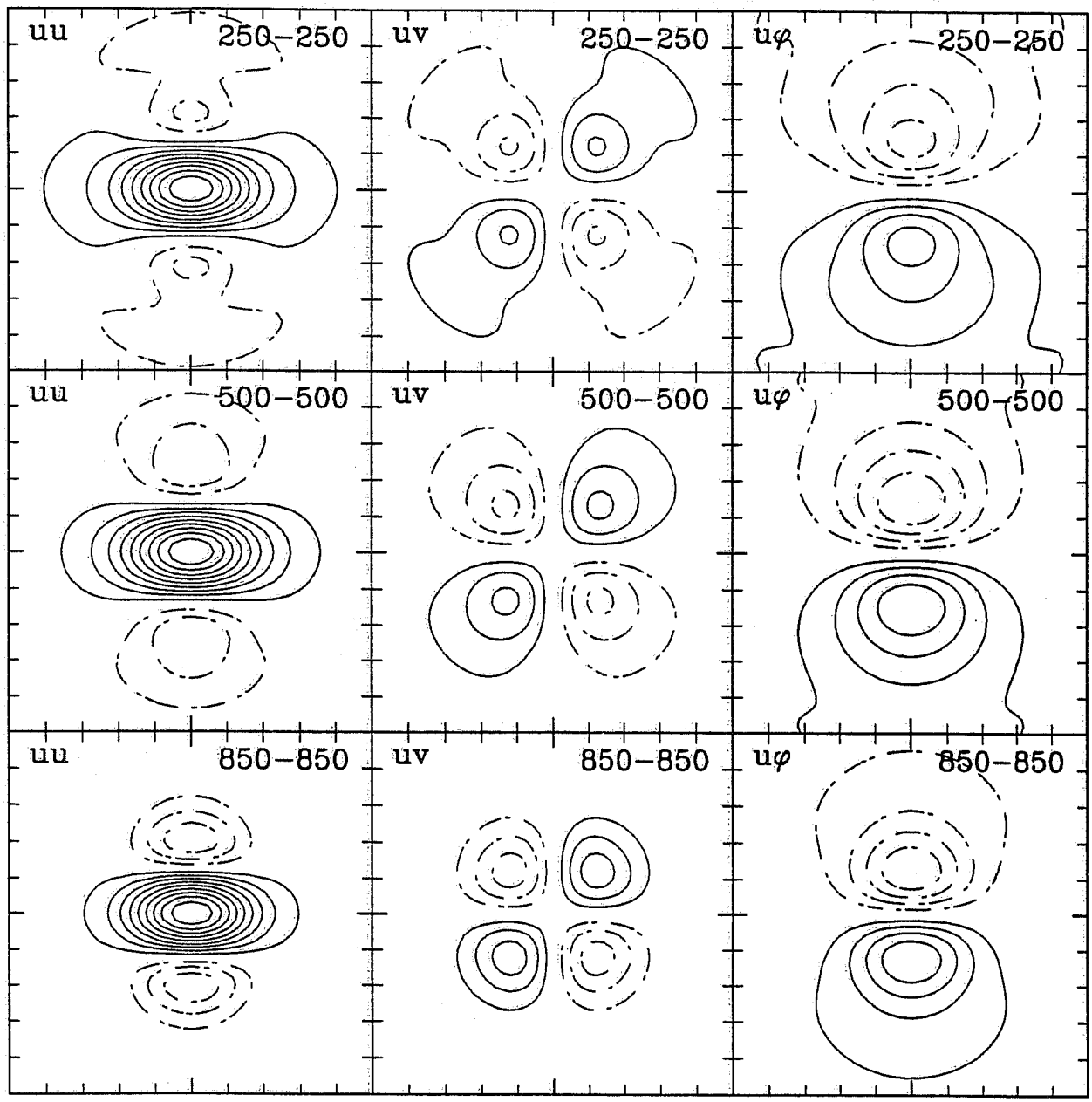

Fig. 4. The *uu*, *uv* and $u\phi$ correlations on the *x-y* plane at 250, 500 and 850 mb, as obtained geostrophically from the geopotential statistics. The contour interval is 0.1, the zero contour has been suppressed and negative contours are represented by dash-dotted lines. Each square is 2500 km by 2500 km.

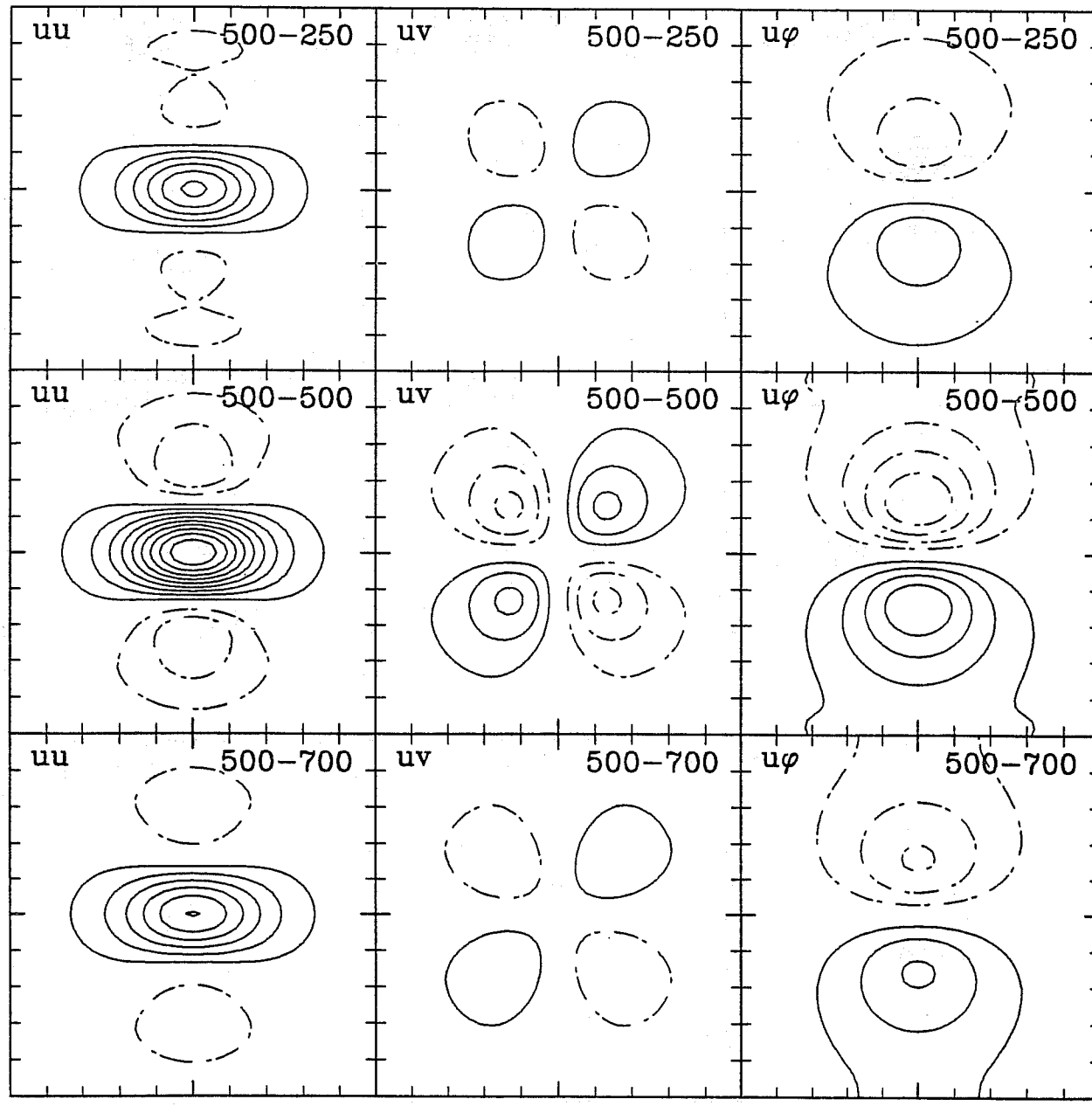

Fig. 5. As in Fig. 4 except that 250, 500 and 700 mb correlations are calculated with respect to a *u*-datum at 500 mb.

2. THE EFFECT OF ASSIMILATING MODEL RESOLUTION ON DATA ASSIMILATION

This study was undertaken to investigate the effect of assimilating model resolution on data assimilation. One aspect of interest is the effect of using a variable-mesh assimilating model. Here we confine our attention to the case of a uniform-mesh model.

2.1 Theory

Consider a one-dimensional periodic domain $-\pi a \le x \le \pi a$. We define the "true" state or signal h(x,t) as a Fourier series truncated at wavenumber K. The signal is assumed to satisfy the one-dimensional linear advection equation,

$$\frac{\partial h}{\partial t} + U\frac{\partial h}{\partial x} = 0, \tag{2}$$

where U is the (constant) advecting velocity. In spectral form,

$$\hat{\mathbf{h}}_{n+1} = \hat{\mathbf{M}}\,\hat{\mathbf{h}}_n \ , \tag{3}$$

where $\hat{\mathbf{h}}_n$ is the vector of length 2K + 1 of Fourier coefficients at time t_n and $\hat{\mathbf{M}}$ is a (2K+1) x (2K+1) matrix.

Consider data assimilation with an assimilating model whose (uniform) mesh is x_j, $1 \le j \le J$. Define $\overline{\mathbf{h}}^a_n$ and $\overline{\mathbf{h}}^f_n$ as the analyzed and forecast values of h on the grid x_j at time t_n. $\overline{\mathbf{h}}^a_n$ and $\overline{\mathbf{h}}^f_n$ are defined to represent only the scales resolvable by the grid, hence the overbar which represents the spatial averaging. The assimilating model on this mesh will be a discrete approximation to the linear advection equation and is a J x J matrix which we denote **M**. Then, the forecast values at time t_{n+1} are obtained from the analyzed values at time t_n by,

$$\overline{\mathbf{h}}^f_{n+1} = \mathbf{M}\,\overline{\mathbf{h}}^a_n \tag{4}$$

We will define the discrete model **M** below.

Consider now a time independent observation network x_i, $1 \le i \le I$, and a column vector of length I of observations $\mathbf{h}^o_n$ on this network at time t_n. We will assume that these observations are radiosonde-like point observations, i.e., they include all wavenumbers $\le K$. Expressions for the analyzed values on the grid x_j of the state variable h at time t_n for the assimilating model can be written,

$$\overline{\mathbf{h}}^a_n = \overline{\mathbf{h}}^f_n + \mathbf{K}_n\left[\mathbf{h}^o_n - \mathbf{H}\,\overline{\mathbf{h}}^f_n\right] \ , \tag{5}$$

where **H** is an I x J time-independent forward interpolation matrix and $\mathbf{K}_n$ is a J x I weight or gain matrix. The vector $\mathbf{r}_n$ (of length I) of observation errors is assumed to be stationary, unbiased and neither spatially nor serially correlated and thus $\mathbf{r}_n$ is only correlated with itself. The instrument

error covariance, $\mathbf{R} = \langle \mathbf{r}_n \mathbf{r}_n^T \rangle$, is time independent and homogeneous since the variance $(E_h^o)^2$ is assumed to be the same at each observation station. $\mathbf{R}$ is also diagonal because $\mathbf{r}_n$ is not spatially correlated thus $\mathbf{R} = (E_h^o)^2\ \mathbf{I}$, where $\mathbf{I}$ is the identity matrix. In the experiments discussed below, we set E^o_h = 10 m.

The signal covariance, $\hat{\mathbf{S}}_n = \langle \hat{\mathbf{h}}_n \hat{\mathbf{h}}_n^T \rangle$, is stationary and is a (2K+1)x(2K+1) diagonal matrix whose elements are spectral variances. This implies that the signal covariance is homogeneous. The elements of $\hat{\mathbf{S}}$ are given by $\langle h^2 \rangle\ \hat{g}(k)$, where $\langle h^2 \rangle$ is the (constant) height variance of the signal and $\hat{g}(k)$ is the Fourier transform (on a continuous, infinite domain) of the correlation function,

$$\rho(x) = \left[\cos(b|x|) + \frac{\sin(b|x|)}{\ell b} \right] \exp(-|x| / \ell) \quad . \tag{6}$$

$\rho(x)$ is the second order autoregression function introduced by Thiébaux (1976). When b = 0, this eqn. simplifies to eqn. (4.8) of Daley (1992). When b = 0, $\rho(x)$ is always greater than zero for finite x, and $\hat{g}(k)$ is a maximum at k = 0. This choice is appropriate for forecast error covariances, but is less appropriate for the signal variance (see Daley, 1991, section 4.3). In these experiments, we set b = 4 / a, ℓ = a / 3 for the signal covariance. $\langle h^2 \rangle$ is specified so that the total signal variance at any point in physical space is 10 000 m^2. In Fig. 6, we plot the spectrum of the signal for these choices.

Define a Fourier transform, $\mathbf{F}$, from spectral space to the grid. $\mathbf{F}$ filters all Fourier components with wavelengths smaller than (j-1)/2. Define $\bar{\mathbf{e}}_n^f = \bar{\mathbf{h}}_n^f - \mathbf{F}\hat{\mathbf{h}}_n$ and $\bar{\mathbf{e}}_n^a = \bar{\mathbf{h}}_n^a - \mathbf{F}\hat{\mathbf{h}}_n$, the forecast and analysis errors on the grid. Define $\bar{\mathbf{P}}_n^f = \langle \bar{\mathbf{e}}_n^f (\bar{\mathbf{e}}_n^f)^T \rangle$ and $\bar{\mathbf{P}}_n^a = \langle \bar{\mathbf{e}}_n^a (\bar{\mathbf{e}}_n^a)^T \rangle$, the forecast and analysis error covariances on the grid. One obtains a forecast error covariance eqn. of the form:

$$\bar{\mathbf{P}}_{n+1}^f = \mathbf{M}\bar{\mathbf{P}}_n^a\mathbf{M}^T + \left[\mathbf{MF} - \mathbf{F}\hat{\mathbf{M}}\right] \hat{\mathbf{S}} \left[\mathbf{MF} - \mathbf{F}\hat{\mathbf{M}}\right]^T + \text{" cross terms"} \tag{7}$$

The second right-hand-side term is the error covariance due to the discretization error of model $\mathbf{M}$. In a similar way, one obtains an analysis error covariance eqn. of the form:

$$\bar{\mathbf{P}}_n^a = [\mathbf{I} - \mathbf{K}_n\mathbf{H}]\, \bar{\mathbf{P}}_n^f\, [\mathbf{I} - \mathbf{K}_n\mathbf{H}]^T + \mathbf{K}_n \left[\mathbf{R} + (\mathbf{G} - \mathbf{HF})\, \hat{\mathbf{S}}\, (\mathbf{G} - \mathbf{HF})^T\right] \mathbf{K}_n^T + \text{"cross terms"} \quad . \tag{8}$$

Here $\mathbf{G}$ is the Fourier transform between the Fourier coefficients and the observation locations. Note the term $[\mathbf{G} - \mathbf{HF}]\, \hat{\mathbf{S}}\, [\mathbf{G} - \mathbf{HF}]^T$, which is an extra component of the observation error covariance. This term is the forward interpolation error covariance due to the forward interpolation error between analysis grid and observation network discussed by Lorenc (1986).

Let $\mathbf{R}^*$ denote the sum of instrument error covariance and forward interpolation error covariance. Then the Kalman gain matrix has the form

$$\mathbf{K}_n = \bar{\mathbf{P}}_n^f\, \mathbf{H}^T \left[\mathbf{H}\bar{\mathbf{P}}_n^f\mathbf{H}^T + \mathbf{R}^*\right]^{-1} \quad . \tag{9}$$

We are interested in the stationary statistics which can be obtained by integrating the second moment equations until stationarity is achieved. There is a difficulty, however. $\overline{\mathbf{P}}_n^f$ and $\overline{\mathbf{P}}_n^a$ are the error covariances corresponding to the scales resolved by the (possibly very coarse) grid of the assimilating model. If the grid is very coarse, then it will only be able to resolve the largest spatial scales of the signal or any error in the signal. Scales too small to be resolved by the mesh will not make any contribution to the errors $\overline{\mathbf{P}}_n^f$ and $\overline{\mathbf{P}}_n^a$. Thus, it is also necessary to consider the errors in the unresolved scales. To do this we introduce $\hat{\mathbf{e}}_n^a$ and $\hat{\mathbf{e}}_n^f$, the *spectral* analysis and forecast errors. Defining $\hat{\mathbf{P}}_n^a = \left(\hat{\mathbf{e}}_n^a\right)\left(\hat{\mathbf{e}}_n^a\right)^T$, the spectral analysis arror covariance matrix, we obtain the following expression for $\hat{\mathbf{P}}_n^a$:

$$\hat{\mathbf{P}}_n^a = \tilde{\mathbf{F}}\overline{\mathbf{P}}_n^a\tilde{\mathbf{F}}^T + \mathbf{U}\,\hat{\mathbf{S}}\,\mathbf{U}^T + \text{"cross terms"} \quad . \tag{10}$$

Here $\tilde{\mathbf{F}}$ is the (2K + 1) x J Fourier transform matrix from the grid x_j to spectral space and U is a diagonal matrix with (in the cases considered here) 1's in the resolved part of the spectrum and 0's in the unresolved part of the spectrum. A similar expression can be derived for $\hat{\mathbf{P}}_n^f$. $\hat{\mathbf{P}}_n^a$ and $\hat{\mathbf{P}}_n^f$ can be transformed to spatial form on any grid by left multiplication by the appropriate Fourier transform matrix and right multiplication by its transpose.

Two assimilating models $\mathbf{M}_1$ and $\mathbf{M}_2$ are considered for the grid x_j, $1 \le j \le J$. The first model is the exact Fourier model (truncated at wavenumber (J-1) / 2) described in Daley (1992). It is defined by,

$$\mathbf{M}_1 = \mathbf{F}\,\hat{\mathbf{M}}\,\tilde{\mathbf{F}} \quad . \tag{11}$$

For this model, the matrix $[\mathbf{MF} - \mathbf{F}\hat{\mathbf{M}}] = \mathbf{F}\hat{\mathbf{M}}(\tilde{\mathbf{F}}\mathbf{F} - \mathbf{I})$ is identically zero and thus there is no model error in the resolved scales which the model handles perfectly. We also define a second model $\mathbf{M}_2$. The linear advection equation has the solution at time $t_{n+1} = t_n + \Delta t$: $h(x,t_{n+1}) = h(x - U\Delta t, t_n)$. This suggests a semi-Lagrangian time marching algorithm. The point of departure $(x-U\Delta t)$ is always known exactly for this equation, so all that is necessary is to interpolate the values of $h(x-U\Delta t)$ from the values of h at the gridpoints of the mesh. This interpolation is performed using periodic cubic splines which pass through the gridpoints of the mesh. We note that in the case of a uniform mesh where the Courant number has been chosen to be an integer, $\mathbf{M}_1 = \mathbf{M}_2$.

2.2 Results with the model $\mathbf{M}_1$

a) Uniform observation network coincides with analysis mesh.

In this case, I = J, $\mathbf{H} = \mathbf{I}$. With this model, which is perfect in the resolved scales since the matrix $[\mathbf{MF} - \mathbf{F}\hat{\mathbf{M}}]$ is zero, the second moment equations reduce to:

$$\overline{\mathbf{P}}_{n+1}^f = \mathbf{M}\,\overline{\mathbf{P}}_n^a\,\mathbf{M}^T \tag{12}$$

$$\overline{\mathbf{P}}_n^a = [\mathbf{I} - \mathbf{K}_n]\,\overline{\mathbf{P}}_n^f\,[\mathbf{I} - \mathbf{K}_n]^T + \mathbf{K}_n\left[\mathbf{R} + (\mathbf{G} - \mathbf{F})\,\hat{\mathbf{S}}\,(\mathbf{G} - \mathbf{F})^T\right]\mathbf{K}_n^T + \text{"cross terms"} \tag{13}$$

The stationary solution of this set of equations is: $\overline{\mathbf{P}}^f = \overline{\mathbf{P}}^a = \mathbf{K} = 0$. It then follows that $\hat{\mathbf{P}}^a = \mathbf{U}\,\hat{\mathbf{S}}\,\mathbf{U}^T$, which is a diagonal matrix, identical to $\hat{\mathbf{S}}$ in the unresolved part of the spectrum and zero elsewhere. Thus $\hat{\mathbf{P}}^a$ consists of error in the unresolved scales only, and the fact that it is diagonal implies that it corresponds to a homogeneous error on the grid.

Set K = 32 so that 2K+1 = 65. Then the analysis error variance on the grid of the assimilating model (i.e., the value of the diagonal elements of $\overline{\mathbf{P}}^a$) for J =45 and J = 15 is represented by the dots in Figs. 7a and 7c, respectively. For J = 45, the variance in the unresolved scales at any point in physical space is 19 m^2 as can be roughly confirmed from Fig. 6. For J = 15, when a much larger fraction of the 10 000 m^2 total signal variance is unresolved, the corresponding value is 792 m^2. Since in the present case the total analysis error consists only of error in the unresolved scales, these values also represent the total analysis error variance. The solid curves in Figs. 7a and 7c represent the latter variance on a high-resolution output grid for J = 15 and J = 45, respectively.

In the previous case we obtained $\mathbf{K} = 0$ so that, according to (5), the analyzed value was set equal to the forecast and the observations were completely disregarded. Suppose now that rather than calculating $\mathbf{K}_n$, we set $\mathbf{K}_n = \mathbf{I}$. This is the opposite extreme since now, according to (5), the analyzed value is set equal to the observed value at each analysis point, completely ignoring the model forecast. Then we obtain the following stationary solution:

$$\overline{\mathbf{P}}^f = \overline{\mathbf{P}}^a = \mathbf{R} + [\mathbf{G} - \mathbf{F}]\,\hat{\mathbf{S}}\,[\mathbf{G} - \mathbf{F}]^T \tag{14}$$

Then

$$\hat{\mathbf{P}}_n^a = \tilde{\mathbf{F}}\left[\mathbf{R} + (\mathbf{G} - \mathbf{F})\,\hat{\mathbf{S}}\,(\mathbf{G} - \mathbf{F})^T\right]\tilde{\mathbf{F}}^T + \mathbf{U}\,\hat{\mathbf{S}}\,\mathbf{U}^T + \text{"cross terms"}\ . \tag{15}$$

We now consider the various terms on the right-hand side of (15).

When transformed to spatial form the instrument error term yields the homogeneous instrument error variance $(E^o{}_h)^2$. The $\tilde{\mathbf{F}}\,(\mathbf{G} - \mathbf{F})\,\hat{\mathbf{S}}\,(\mathbf{G} - \mathbf{F})^T\,\tilde{\mathbf{F}}^T$ term represents the forward interpolation covariance in spectral form. The effect of left multiplying the diagonal matrix $\hat{\mathbf{S}}$ by $\tilde{\mathbf{F}}\,(\mathbf{G} - \mathbf{F})$ and right-multiplying by its transpose is to "fold back" the elements of $\hat{\mathbf{S}}$ around the Nyquist scale from the unresolved to the resolved part of the spectrum. This yields a diagonal matrix only the first J diagonal elements of which can be non-zero. Fig. 8 shows the spectrum of $\tilde{\mathbf{F}}\,(\mathbf{G} - \mathbf{F})\,\hat{\mathbf{S}}\,(\mathbf{G} - \mathbf{F})^T\,\tilde{\mathbf{F}}^T$ for J = 45 and 35, which clearly illustrate this "fold back" of covariance error. Also shown in Fig. 8 are the corresponding spectra for J = 25 and 15. In these cases, as 2K+1-J > J, we see the error from more than one unresolved wave being aliased onto the same resolved wave. The error in the resolved scales due to the misrepresentation of scales which the observation network is unable to

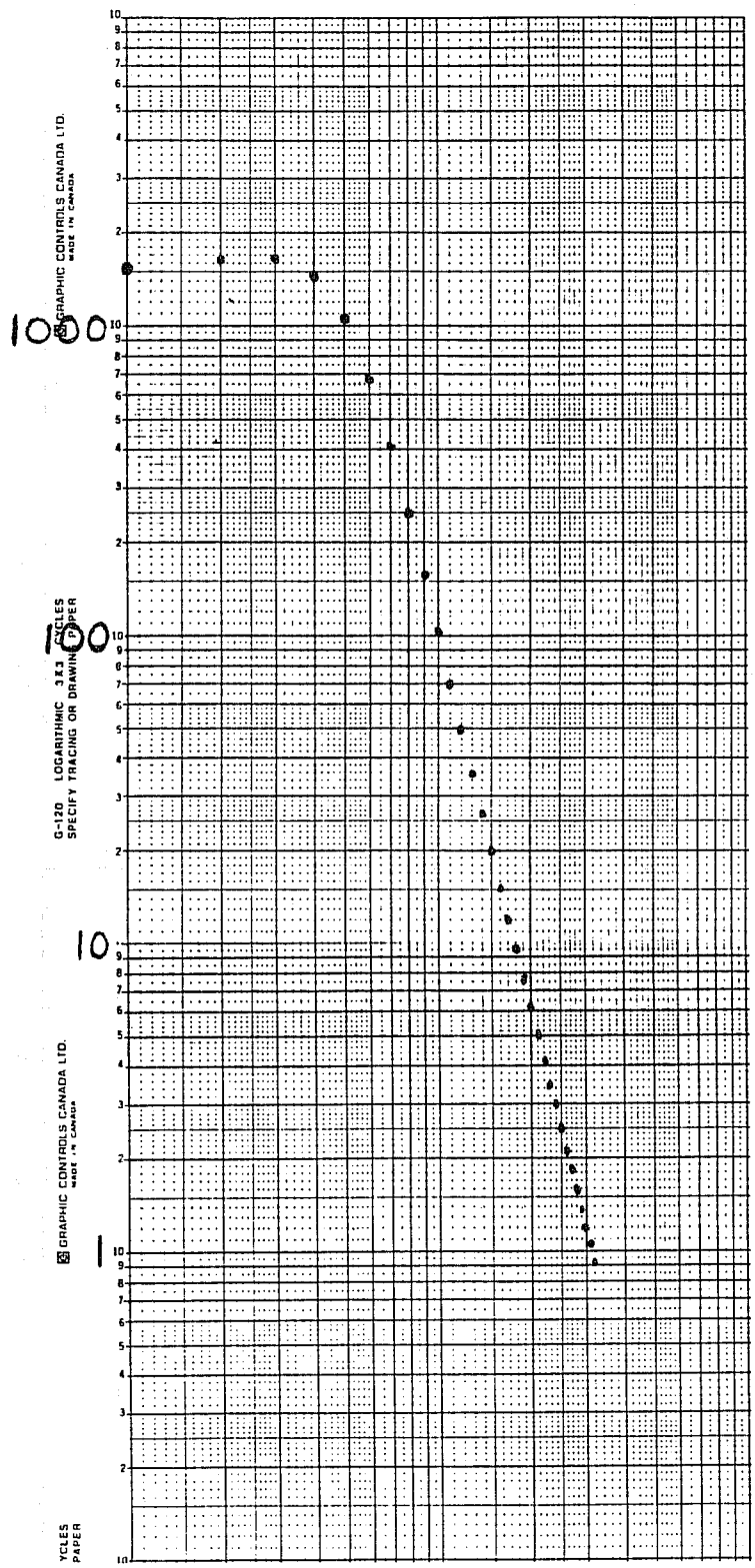

Fig. 6. The spectrum of the signal.

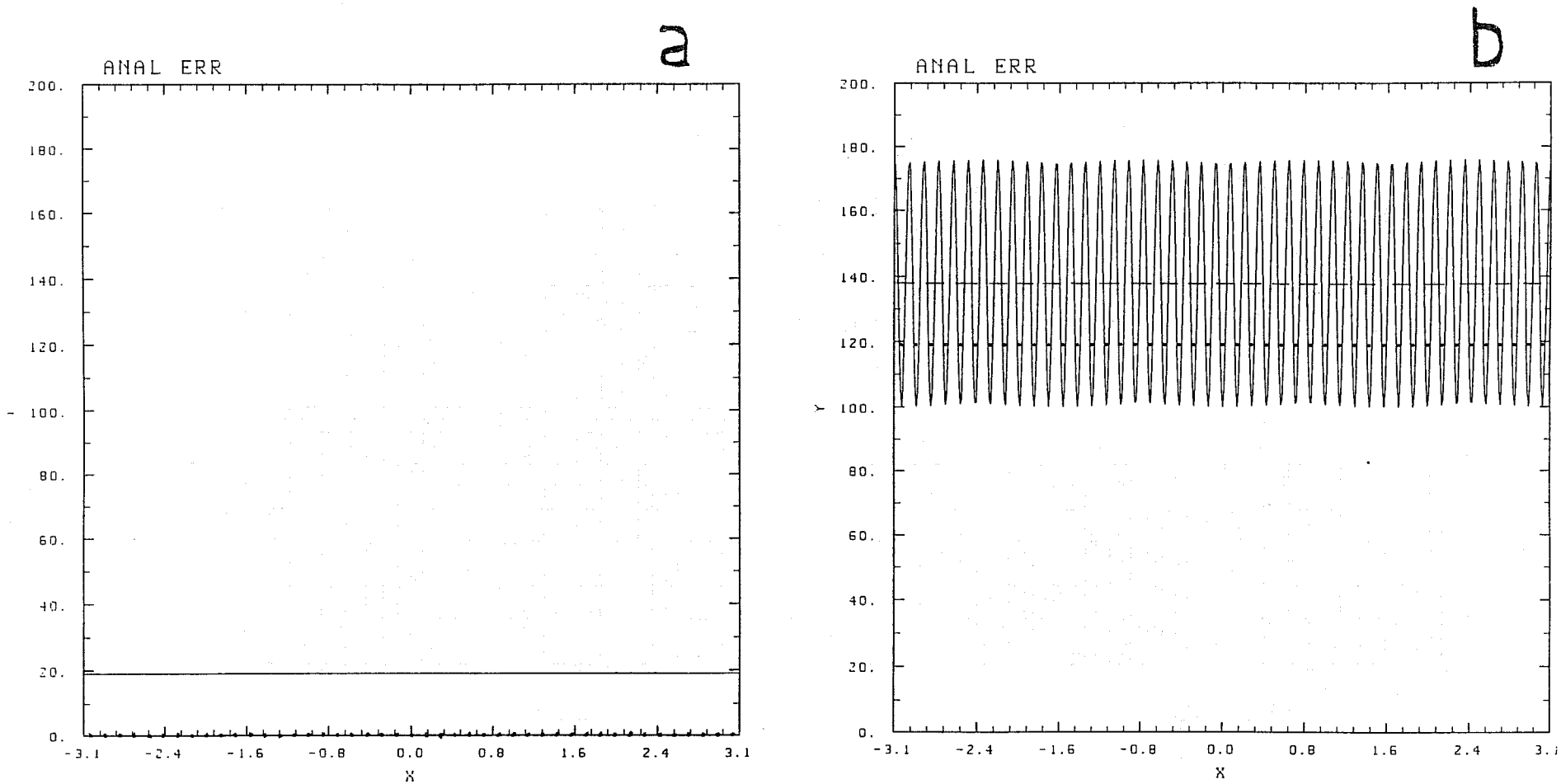

Fig. 7. In each panel, the dots represent the analysis error variance on the grid (i.e., the diagonal elements of $\bar{\mathbf{P}}^{a)}$) and the solid line represents the total analysis error on a high-resolution output grid. Note that the horizontal distance along the abscissa is given in non-dimensional units. Panel (a): J = 45, **K** (the Gain matrix) = 0. Panel (b): As in panel (a) except **K** (the Gain matrix) = **I** (the identity matrix). Panel (c): J = 15, **K** (the Gain matrix) = 0. Panel (d): As in panel (c) except **K** (the Gain matrix) = **I** (the identity matrix).

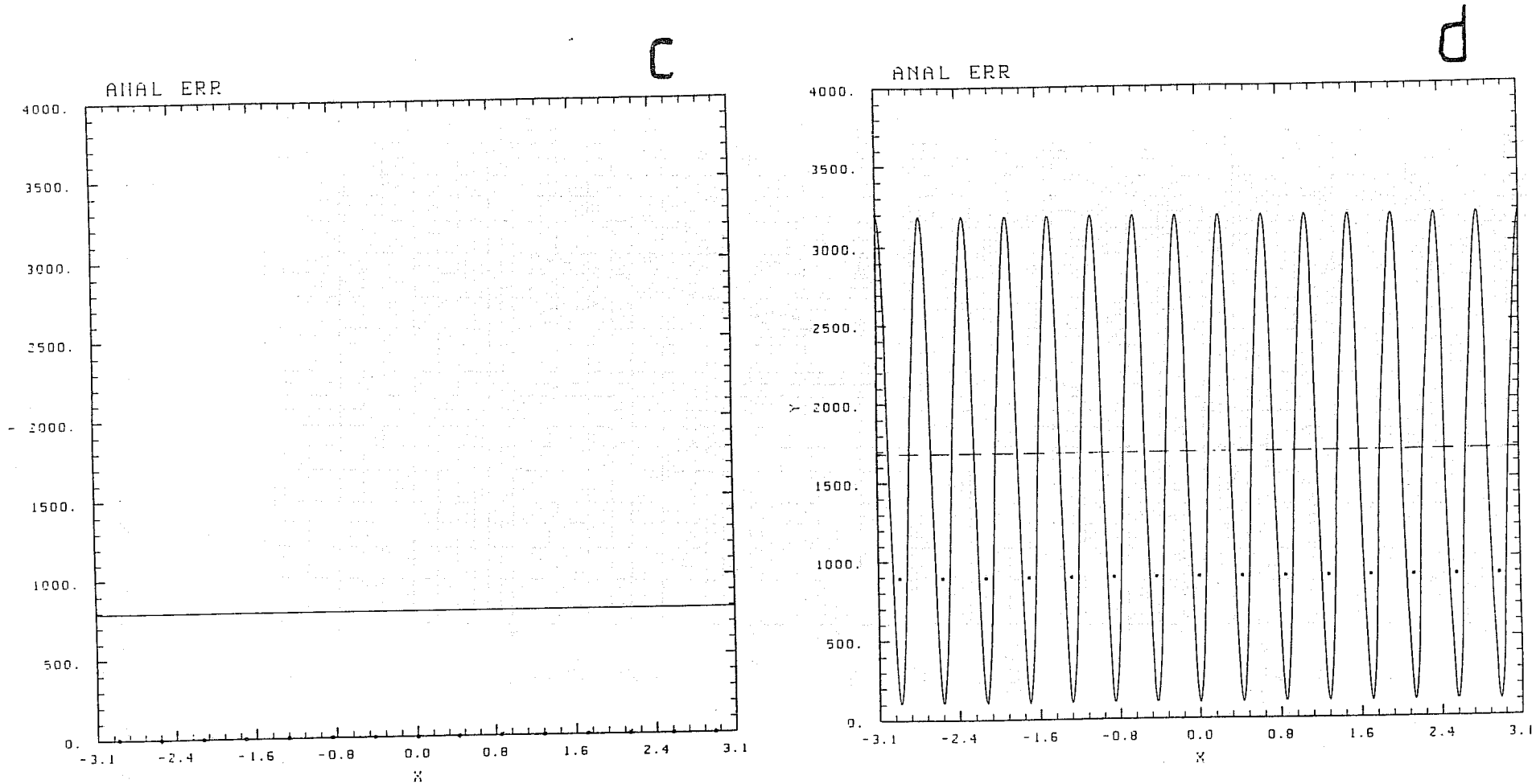

Fig. 7. Panels (c) and (d).

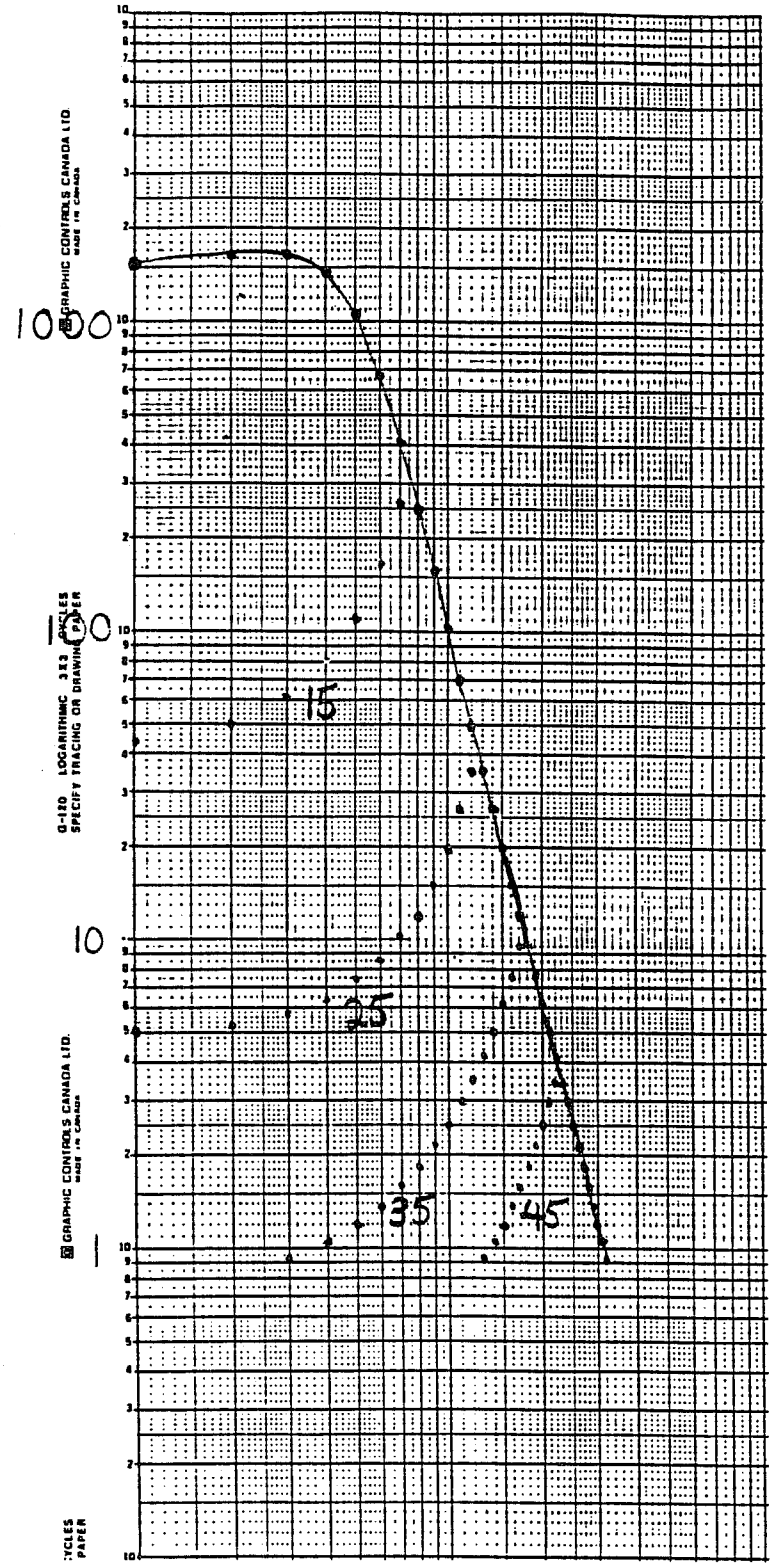

Fig. 8. The spectrum of the signal as in Fig. 6. Also shown are the spectra of the forward interpolation error term for J= 15, 25, 35 and 45.

resolve is a type of observation error commonly referred to as the "error of representativeness" (e.g., Daley 1991). Returning to (14), we see that $\bar{\mathbf{P}}^a$ (= $\bar{\mathbf{P}}^f$) consists of instrument error and error of representativeness only.

By contrast, the right-hand side of (15) contains additional terms. The $\mathbf{U}\,\mathbf{S}\,\mathbf{U}^T$ is the error in the unresolved scales, as before. It, like the previous terms, is a diagonal matrix. Thus, when transformed to spatial form, these terms give rise to homogeneous error covariances. Furthermore, because the forward interpolation error is a "folded back" image of the error in the unresolved scales, it and the unresolved error contribute equally to the total analysis error variance in spatial form.

The dots in Fig.7b are the analysis error variance on the grid of the assimilating model (i.e., the diagonal elements of $\bar{\mathbf{P}}^a$) for the case J = 45. These have a value of 119 (= 100 + 19) m^2. The dashed line in the figure is the homogeneous portion of the total analysis error variance on a high-resolution output grid. This has a value of 138 (= 100 + 19 + 19) m^2. The solid curve represents the total analysis error variance on the high-resolution output grid. We see that the effect of the cross terms is to introduce a sinusoidal oscillation with amplitude 38 m^2. This oscillation reduces the error variance to 100 m^2 (the instrument error) at each point of the analysis grid, consistent with our specification of the gain matrix **K**. However the analysis error now reaches a maximum value of 176 m^2 mid-way between points of the analysis grid. All of these values are much larger than those obtained in the case of an optimal gain matrix, where the total analysis error variance was only 19 m^2.

The corresponding curves for the case J = 15 are shown in Fig. 7d where the situation is seen to be entirely analogous: the diagonal elements of $\bar{\mathbf{P}}^a$ are now 892 (= 100 + 792) m^2, the homogeneous portion of the total analysis error variance on the high-resolution output grid has a value of 1684 (= 100 + 792 + 792) m^2, and in order to reduce the error variance to 100 m^2 (the instrument error) at each point of the analysis grid, the sinusoidal oscillation due to the inhomogeneous terms now has an amplitude of 1584 (= 2x792) m^2.

We note that whether the gain matrix $\mathbf{K}_n$ was calculated using (5) ("the perfect model case") or set equal to **I** (the "no-model" case), the expressions we obtained for $\bar{\mathbf{P}}^a$ and $\hat{\mathbf{P}}^a$ did not involve **M**. It follows that these results are valid independently of our choice of Courant number. The perfect model and no-model cases are important as they constitute extremes at opposite ends of the range of behaviours exhibited by more common (imperfect) models.

b) Non-uniform observation network.

In this case the second moment equations reduce to the same equations as before, except that in (13) the terms $[\mathbf{I} - \mathbf{K}_n]$ and $[\mathbf{G} - \mathbf{F}]$ must be replaced by the more general $[\mathbf{I} - \mathbf{K}_n \mathbf{H}]$ and $[\mathbf{G} - \mathbf{H}\,\mathbf{F}]$ respectively. As before, the stationary solution is: $\bar{\mathbf{P}}^f = \bar{\mathbf{P}}^a = \mathbf{K} = 0$. Again it follows that $\hat{\mathbf{P}}^a = \hat{\mathbf{P}}^f = \mathbf{U}\,\hat{\mathbf{S}}\,\mathbf{U}^T$. Thus for this perfect model, the second moment equations yield an analysis error which is completely independent of the observations, of their location, of their observational error and even of their number. As before, these results are not dependent on our choice of Courant number.

2.3 Conclusions

The results presented above have focused on the error in the unresolved scales and its effect on the forward interpolation error. More complete results, which include the effect of non-zero model discretization error (i.e., $[\mathbf{MF} - \mathbf{F}\hat{\mathbf{M}}] \neq 0$), will be found in Mitchell and Daley (1992).

REFERENCES

Bartello, P., and H.L. Mitchell, 1992: A continuous three-dimensional model of short-range forecast error covariances. *Tellus,* **44A**, 217-235.

Daley, R., 1991: *Atmospheric Data Analysis,* Cambridge University Press, Cambridge, 457 pp.

Daley, R., 1992: The lagged innovation covariance: a performance diagnostic for atmospheric data assimilation. *Mon. Wea. Rev.*, **120**,.178-196.

Gandin, L.S., 1963: *Objective analysis of meteorological fields*. Translated from Russian by the Israeli Program for Scientific Translations (1965).

Hollingsworth, A., and P. Lönnberg, 1986: The statistical structure of short-range forecast errors as determined from radiosonde data. Part I: The wind field. *Tellus*, **38A**, 111-136.

Lönnberg, P., and A. Hollingsworth, 1986: The statistical structure of short-range forecast errors as determined from radiosonde data. Part II: The covariance of height and wind errors. *Tellus*, **38A**, 137-161.

Lorenc, A., 1986: Analysis methods for numerical weather prediction. *Quart. J. Roy. Meteor. Soc.*, **112**, 1177-1194.

Mitchell, H.L., C. Charette, C. Chouinard, and B. Brasnett, 1990: Revised interpolation statistics for the Canadian data assimilation procedure: Their derivation and application. *Mon. Wea. Rev.*, **118**, 1591-1614.

Mitchell, H.L., and R. Daley, 1992: The effect of assimilating model resolution on data assimilation (in preparation).

Phillips, N.A., 1986: The spatial statistics of random geostrophic modes and first-guess errors. *Tellus*, **38A**, 314-332.

Rutherford, I.D., 1972: Data assimilation by statistical interpolation of forecast error fields. *J. Atmos. Sci.*, **29**, 809-815.

Thiébaux, H.J., 1976: Anisotropic correlation functions for objective analysis. *Mon. Wea. Rev.*, **104**, 994-1002.